CrossMark

ORIGINAL PAPER

Theoretical and experimental study of the stiffness of electrospun composites of poly(vinyl alcohol), cellulose nanofibers, and nanohydroxy apatite

Mohammad Saied Enayati · T. Behzad · P. Ł. Sajkiewicz · R. Bagheri · L. Ghasemi-Mobarakeh · F. Pierini

Abstract The present study aims to theoretically model and verify the mechanical behavior of electrospun fibers of poly(vinyl alcohol) (PVA) reinforced by nanohydroxy apatite (nHAp) and cellulose nanofibers (CNF), the three composites designated as PVA/nHAp, PVA/CNF, and PVA/nHAp/CNF. Tensile tests and AFM nanoindentation studies were used to measure tensile modulus of electrospun scaffolds and single fibers respectively. Halpin–Tsai and Ouali models were applied to predict the stiffness of electrospun mats. Theoretical analysis according to the Halpin–Tsai model showed that CNF have no preferred orientation in the electrospun fibers, particularly at higher filler content. Additionally, this model provided a better prediction than Ouali model, especially at lower filler content. Theoretical models based on the geometry of an unit cell in open-cell structure such as honeycomb, tetrakaidecahedron and cube models simulate electrospun scaffolds. Among the structural models for analysis of porous scaffolds, the honeycomb model showed the best prediction, tetrakaidecahedron model—a moderate one, and cube model was the worst. In general, it was proved by both experiment and theory that the porous structure of electrospun mat caused significant modulus reduction of nanocomposites.

Keywords Nanocomposites · Cellulose nanofibers · Electrospinning · Modulus

Introduction

In the last decade, electrospun scaffolds have attracted attention due to their high porosity and controllable morphology, as well as the use of simple and low cost equipment during their production (Neisiany et al. 2017a; Persano et al. 2013). Tissue engineering is one of the areas in which electrospun scaffolds are being widely studied because their well-connected structures resemble the extracellular matrix in body tissues (Costa-Júnior et al. 2009). The mechanical properties of scaffolds are extremely important for biomedical applications; however, most of the publications are limited only to experimental measurements (Abdalkarim et al. 2017; Khalf et al. 2015; Linh and Lee 2012; Neisiany et al. 2017b). Analyzing the mechanical behavior of nonwoven fibers and verifying them with the available mechanical models can open the door for

M. S. Enayati · T. Behzad (✉) · R. Bagheri
Department of Chemical Engineering, Isfahan University of Technology, 84156-83111, Isfahan, Iran
e-mail: tbehzad@cc.iut.ac.ir

M. S. Enayati · P. Ł. Sajkiewicz · F. Pierini
Institute of Fundamental Technological Research, Polish Academy of Sciences, Pawinskiego 5B, 02-106 Warsaw, Poland

L. Ghasemi-Mobarakeh
Department of Textile Engineering, Isfahan University of Technology, 84156-83111, Isfahan, Iran

prediction of mechanical properties of electrospun scaffolds (Kumar and Rawal 2017). Consequently, the required amount of reinforcements in polymeric matrix can be estimated before scaffold fabrication.

In order to simulate the mechanical behavior of an element, its geometrical structure must be initially considered. In the case of an electrospun scaffold (Fig. 1a); its architecture resembles an interconnected structure of fibers, which have a random alignment. From another point of view, an electrospun scaffold consists of a series of connected pores (highly porous structure), even to the depth of scaffold, similar to open-celled foam (Fig. 1b). According to the definition, polymeric foams can be considered as a composite of polymer matrix and dispersed gas bubbles or cells. Open-celled foam is defined as a structure in which cells are interconnected throughout its bulk (Lee and Ramesh 2004). Several models have been used to predict the modulus of open-celled foams basing on the porosity of the foams (Shulmeister 1998). Therefore, these models are a reliable approach to analyze the mechanical behavior of electrospun scaffolds.

Taking a deeper look into an electrospun scaffold, it is a network of many submicron- or nano-fibers. Hence, in the case of using a reinforcing agent, a single fiber can be considered as a nanocomposite named as a single fibrous nanocomposite (Fig. 1c). Based on the type of filler, e.g. particles or short fibers, related models can be applied to predict mechanical properties of a fiber. Direct measurement of single fiber mechanical properties is challenging, since isolating and controlling the experimental conditions of

nanosized electrospun fibers are difficult. Several techniques including nanoindentation (Baji et al. 2010; Wang and Barber 2012), AFM nanoindentation (Tan et al. 2005), AFM three-point bend test (Stachewicz et al. 2012; Tan and Lim 2004), and nano-tensile test (Bazbouz and Stylios 2010; Inai et al. 2005) have been used to measure the mechanical properties of single electrospun fibers. In the present study, AFM nanoindentation was used to directly measure Young's modulus of nanofibers.

Some advantages such as biocompatibility, water solubility, hydrophilicity, and nontoxicity of electrospun poly(vinyl alcohol) (PVA) fibers resulted in a great deal of attention directed towards their applications in new areas, such as biomedical and membrane (Adibzadeh et al. 2014; Agrawal and Pramanik 2016; Yang et al. 2008). However, low stiffness of PVA limits its applications, particularly in hard tissue engineering. Because electrospun fibers have submicron diameters, it necessitates the incorporation of nano-scale fillers to produce electrospun PVA nanocomposites. Various nano-sized fillers such as nanohydroxy apatite (nHAp) (Degirmenbasi et al. 2006; Kim et al. 2008; Sheikh et al. 2010), nanosilver (Dong et al. 2010), calcium carbonate (Sambudi et al. 2015), biphasic calcium phosphate (Linh et al. 2013), bioactive glass (Pon-On et al. 2014), zeolite and silica nanoparticles (Mehrasa et al. 2016), nanoclays (Islam et al. 2015; Koosha et al. 2015; Liu et al. 2014), titanium dioxide (Shokrollahi et al. 2014), graphene oxide (Barzegar et al. 2015; Wang et al. 2013), γ-Fe_2O_3 (Fallahiarezoudar et al. 2015), and cellulose nanomaterials (Lee and Deng 2013; Ma et al. 2014;
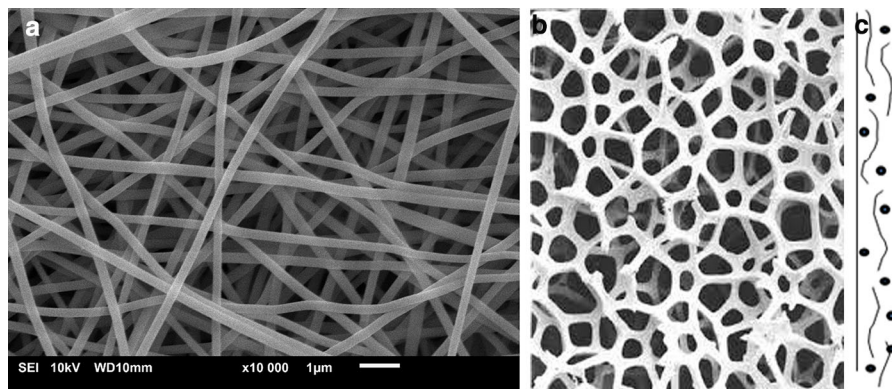

Fig. 1 Two different views of an electrospun fibrous network (**a**), open-celled structure (**b**), and a series of single fibrous nanocomposites (**c**)

Xiao et al. 2016) have been successfully incorporated into electrospun PVA fibers. Electrospun nanocomposites of PVA with two different nanofillers i.e. nanohydroxy apatite and cellulose nanofibers were successfully developed in our previous studies (Enayati et al. 2016a, b).

The aim of the current work is to investigate the mechanical properties of electrospun PVA and its nanocomposites containing nHAp and CNF individually and simultaneously. Then, the experimental measurements are compared with the predictions obtained using theoretical models to prove the accuracy of these models. Considering the PVA nanocomposite as a single fiber, modified Halpin–Tsai (Halpin 1992; Ramakrishna et al. 2006) and Ouali (Ouali et al. 1991; Pooyan et al. 2012) models are used to predict the Young's modulus of CNF-reinforced PVA (as a short-fiber reinforced composite). In the case of nanocomposites containing both nHAp and CNF, since there is not any model to predict the stiffness of a three-component composite, PVA and nHAp are assumed as matrix and CNF as short-fiber reinforcement. Since the synthesized nHAps are in particle form, therefore their better dispersion in PVA matrix and also expected interactions between them and PVA either by hydrogen bonding or [OH–]-Ca^{2+}-[–OH] linkages (Degirmenbasi et al. 2006; Kim et al. 2008; Lee and Deng 2013), this assumption can be acceptable. Electrospun scaffold is considered as an open-celled structure of highly porous nonwoven fibrous nanocomposites and therefore some mechanical models are applied to estimate the Young's modulus of interconnected porous structure. In such models, the modulus of porous structure is proportional to the porosity and modulus of dense (nonporous) material. It is believed that although the presence of high porosity in electrospun scaffolds dramatically reduced the stiffness, the nanofiller reinforcements could compensate for such a reduction.

Experimental

Materials and samples preparation

Polymer

Poly(vinyl alcohol) was supplied by Sigma-Aldrich Company (USA). Its molecular weight and degree of hydrolysis were 124,000 g/mol and 98–98.8% respectively.

Cellulose nanofiber (CNF) extraction

The CNFs were extracted from wheat straw with a chemo-mechanical procedure, as described in our earlier work (Enayati et al. 2016a). Chemicals used during the isolation process including sodium hydroxide (NaOH) granules, hydrochloric acid (HCl) 37 wt%, sodium chlorite ($NaClO_2$) 25 wt%, sulfuric acid (H_2SO_4) 97 wt%, and potassium permanganate flakes ($KMnO_4$), were supplied by Merck (Germany).

Nanohydroxy apatite (nHAp) synthesis

Nanohydroxy apatite, grain size of 15 ± 1 nm, was supplied by Institute of High Pressure Physics, Polish Academy of Sciences (Poland).

PVA, PVA/nHAp PVA/CNF, and PVA/nHAp/CNF nanofiber preparation

PVA solution and its suspensions i.e. PVA/nHAp, PVA/CNF, and PVA/nHAp/CNF were prepared in 80 °C distilled water for 90 min. Next, prepared samples were electrospun. Applied voltage, collection distance, solution rate and needle inner diameter were 18 kV, 15 cm, 700 μL/h and 0.34 mm, respectively. A detailed description of the nanofiber fabrication procedure was presented earlier (Enayati et al. 2016a). Samples containing different amount of nanofillers were coded such as PVA8/nHAp10/CNF3, which means a suspension containing 10 wt% of nHAp and 3 wt% of CNF in a 8 wt% PVA aqueous solution.

Nanofiber characterization

Scanning electron microscopy (SEM)

The spun nanofibers were coated with a thin layer of gold and their morphology was analyzed with scanning electron microscope (SEM, JEOL, JSM-6390LV, Japan) at an accelerating voltage of 10 kV.

Field emission scanning electron microscopy (FE-SEM)

FE-SEM microscope Zeiss Ultra Plus GEMINI (Germany) was used to measure cellulose nanofibers diameter. Prior to observations, samples were coated with a carbon layer. Observations were conducted at accelerating voltage of 2 and 3 kV with SE detector.

Porosity measurement

Porosity (φ) of the electrospun samples was calculated by comparing the apparent density (ρ) to the bulk density of the scaffolds. Rectangular samples were cut from the electrospun mats and their length, width and thickness were accurately measured to determine the volume (V). The dry weight of the samples (m) was measured with an analytical balance with the accuracy of 10^{-4} g. The density of each sample was calculated from its volume and weight according to Eq. (1).

$$\rho = \frac{m}{V} \qquad (1)$$

The porosity, φ, was calculated from the measured average density of the samples, ρ, and the bulk density, ρ_o, from Eq. (2) (Meng et al. 2010).

$$\varphi = \left(1 - \frac{\rho}{\rho_0}\right) \times 100 \qquad (2)$$

AFM nanoindentation

The nanomaterial stiffness was directly measured by AFM nanoindentation analysis. A Ntegra (NT-MDT, Russia) AFM was used to quantify the Young's modulus of the samples. The microscope was equipped with a single crystal silicon cantilever (NSG01, NT-MDT, Russia) with nominal tip radius of 10 nm during the nanocellulose analysis. The spring constant of the previously calibrated cantilever was 11.16 N/m while the sample deposition was carried out by drop casting of the nanocellulose dispersion onto a freshly cleaved mica surface.

The AFM nanoindentation analysis was also performed to locally measure the Young's modulus of single electrospun fibers. A NSG01 cantilever with spring constant of 2.13 N/m was mounted on the AFM head to probe the electrospun fibers and the samples

were prepared by placing a few electrospun fibers onto a mica slide.

At the beginning, the cantilever sensitivity calibration was required (for both sample types) by indenting a clean area of the mica substrate before stiffness measurements. In addition, the slope of the linear signal was recorded when the cantilever is in contact with the reference surface. Furthermore, the tip of the used cantilever was characterized before the indentations as well as after the analyses by SEM and test silicon grating scanning (TGT1, NT-MDT) in order to test their morphological and structural integrity. The AFM topography of the samples surface was collected before each indentation set of measurements. The images were obtained using the described setup operating in tapping contact mode. The selected nanomaterials were analyzed in several zones by collecting a series of force curves. At least 25 indents were performed on each fiber and five different fibers were analyzed for every sample. All the recorded force curves were exported and analyzed. The raw data (cantilever deflection–piezo movement graphs) were converted into applied load force versus indentation depth curves by using the calculated cantilever spring constants and deflection sensitivities. The Young's moduli were evaluated analyzing the loading curves slope and finally the average value was calculated by taking into consideration all the recorded measurements for each sample. In this work, the indented single nanomaterials were treated as a cylinder and the AFM tip as a sphere (Pierini et al. 2016). The nanofibers Young's modulus (E) was calculated by fitting the Hertz model into the loading data using Eq. (3)

$$E = E_r \left(1 - v_f^2\right) \qquad (3)$$

where v_f is the Poisson's ratio of the material and E_r is the relative elastic modulus. The relative elastic modulus is defined by Eq. (4).

$$E_r = \sqrt{\frac{9P^2}{16R_e\delta^3}} \qquad (4)$$

where P is the force applied, δ is the indentation depth, and R_e is the equivalent radius for a spherical indenter evaluated by Eq. (5).

$$R_e = \sqrt{\frac{R_t^2 R_f}{R_t + R_f}} \qquad (5)$$

where R_t is the tip radius of curvature and R_f is the radius of the nanomaterials.

Tensile test

The tensile modulus (E) of electrospun non-woven mats was determined from stress–strain plots obtained from tensile test using uniaxial extension (Instron 4205, USA). The load cell, gauge length, and extension rate were 50 N, 20 mm, and 10 mm/min, respectively. The dimensions of samples were 5 mm (length) × 40 mm (width) × 100 µm (thickness).

Results and discussion

Characterization of extracted cellulose fibers

After chemo-mechanical treatment on wheat straw, observation of final product by FE-SEM confirmed the successful isolation of cellulose nanofibers with average diameter of 30 nm. Detailed results are available in our previous work (Enayati et al. 2016a).

Characterization of electrospun mats

Figure 2 shows the SEM images of electrospun pure PVA (Fig. 2a), and its nanocomposites containing 10 wt% nHAp (Fig. 2b), and 10 wt% nHAp and 3 wt% CNF (Fig. 2c). Smooth fibers of pure PVA change to more irregular after addition of both nanofillers. Moreover, nanofiller incorporation leads to fiber diameter reduction. The complete results and

discussion on fiber morphology and diameter can be found in our previous works (Enayati et al. 2016a, b).

Table 1 lists the average fiber diameter and porosity of electrospun mats. According to the Table 1, all samples show high porosity, more than 70%, which is an important parameter for tissue engineering applications. Although the highest porosity content belongs to pure PVA fiber mat, addition of fillers slightly reduced the porosity which is in accordance with fiber diameter reduction (Meng et al. 2010).

Mechanical behavior

In the previous work, it was shown that PVA/nHAp nanocomposites that incorporated with 1 and 10 wt% of nanoparticles had higher stiffness (Enayati et al. 2016a), therefore these samples were selected for adding different amounts of CNF. Figure 3 displays the effect of CNF content on elastic modulus of nanocomposites with two different nHAp contents.

As it can be observed, PVA8/nHAp1 and PVA8/nHAp10 reinforced with 5 and 3 wt% of CNF, respectively, show the largest modulus in each nanocomposite group. Detailed explanation of such trend has been presented previously (Enayati et al. 2016a). According to the obtained mechanical stiffness, PVA8/nHAp1/CNF5 and PVA8/nHAp10/CNF3 were chosen for more mechanical analysis. In addition, for comparison, samples of PVA8/CNF3 and PVA8/CNF5 were electrospun and mechanically characterized.

In order to study the reinforcement effect of nanofillers, the moduli of the CNF and electrospun single fibers were measured using a nanoindenter (Table 2). Cellulose nanofibers have modulus 40 ± 4.05 GPa, which is in agreement with results reported by Usov et al. (2015). Low modulus of pure
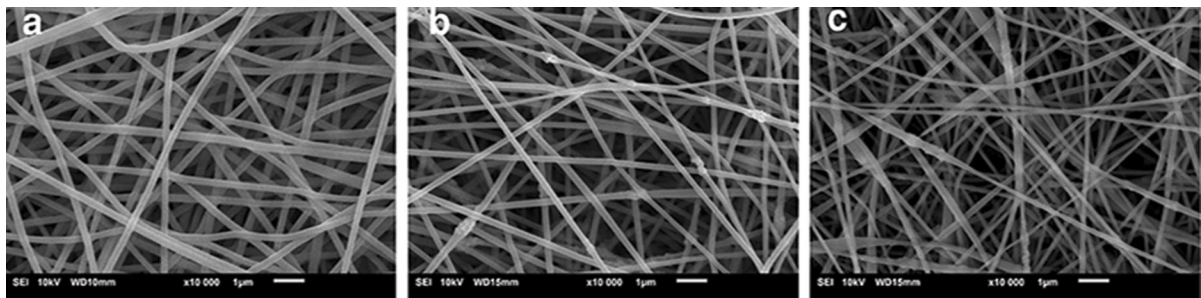

Fig. 2 SEM images of electrospun: **a** PVA8, **b** nHAp8/nHAp10, **c** PVA8/nHAp10/CNF3

Table 1 Fiber diameter and porosity of electrospun PVA and its nanocomposites

Sample	Average diameter (nm)	Porosity (%)
PVA8	228 ± 38.39	80.4 ± 1.63
PVA8/nHAp1	219 ± 32.33	79.84 ± 1.25
PVA8/nHAp10	140 ± 46.58	79.02 ± 1.66
PVA8/CNF3	161 ± 45.46	76.54 ± 1.23
PVA8/CNF5	150 ± 40.78	76.10 ± 0.95
PVA8/nHAp1/CNF5	131.48 ± 37.7	78.65 ± 1.15
PVA8/nHAp10/CNF3	145.63 ± 36.83	75.39 ± 0.84
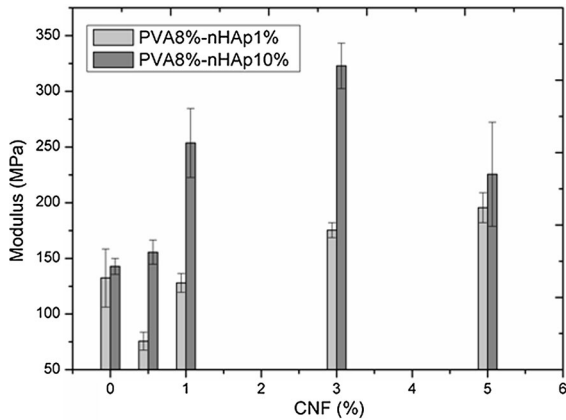
Fig. 3 Effect of CNF loading on elastic modulus of PVA8/nHAp1 and PVA8/nHAp10

Table 2 Modulus of nanocomposites determined by nanoindentation method

Sample	Nanoindentation modulus (GPa)
CNF	40 ± 4.04
PVA8	1.7 ± 0.28
PVA8/nHAp1	12.73 ± 3.5
PVA8/nHAp10	15.74 ± 2.84
PVA8/CNF3	2.57 ± 0.59
PVA8/CNF5	3.37 ± 0.47
PVA8/nHAp1/CNF5	14.36 ± 2.72
PVA8/nHAp10/CNF3	17.34 ± 3.46

electrospun PVA (1.7 GPa for PVA8) was increased by 44 and 90% after incorporation of 3 and 5 wt% of CNF, respectively. It was reported by Lee (Lee and Deng 2013) that stiffness of PVA/cellulose nanowhisker electrospun fibers was linearly increased by increasing cellulose nanowhisker contents. The same trend was also observed in this study. Nanoindentation of PVA nanocomposites containing nHAp shows

much higher stiffness as 12.73 GPa for 1 wt% nHAp and 15.74 GPa for 10 wt% nHAp. The addition of CNF to nHAp/PVA nanocomposites also raised the stiffness by approximately 10%.

Analysis of single-fiber nanocomposite: comparison with theoretical models

Two theoretical models were applied to predict the stiffness of CNF-loaded nanocomposites and their outcomes were compared with the experimental results to verify the accuracy of models.

Halpin–Tsai model (Halpin 1992) has been widely used to predict modulus of short-discontinuous fiber filled composites. The main assumption of this model is that there is no filler–filler interaction Similar to any other micromechanical model, Halpin–Tsai model attempts to estimate the composite modulus based on the modulus of the reinforcement and matrix materials, as well as the shape and volume fraction of the aligned inclusion phase. Based on the orientation of the fibers toward the tensile test direction, longitudinal, transverse, and isotropic Halpin–Tsai models can be applied.

According to these models, longitudinal modulus (E_L) is calculated from Eq. (6).

$$E_L = E_m \frac{1 + \zeta \eta_L v_f}{1 - \eta_L v_f} \tag{6}$$

where E_m and E_f are modulus of matrix and fibers, v_f is fiber volume fraction, and η_L and ζ (aspect ratio) are defined from Eqs. (7) and (8), respectively.

$$\eta_L = \frac{\frac{E_f}{E_m} - 1}{\frac{E_f}{E_m} - \zeta} \tag{7}$$

$$\zeta = 2\frac{l}{d} \tag{8}$$

where l and d are length and diameter of CNF, respectively.

In transverse Halpin–Tsai model $\zeta = 2$ so the model is explained by Eq. (9).

$$E_T = E_m \frac{1 + 2\eta_T v_f}{1 - \eta_T v_f} \tag{9}$$

$$\eta_T = \frac{\frac{E_f}{E_m} - 1}{\frac{E_f}{E_m} - 2} \tag{10}$$

Isotropic Halpin–Tsai model is fractional summation of both E_L and E_T (Eq. 11).

$$E = \frac{3}{8}E_L + \frac{5}{8}E_T \tag{11}$$

To predict the elastic modulus of composites, another model was derived by Ouali (Ouali et al. 1991). This model considers the behavior of an incomplete set of interconnected elements and allows the transition from a local to an infinite communication state where the critical volume fraction or percolation threshold separates the two phases. This model assumed formation of rigid structure when interconnections between series of elements (here, cellulose nanofibers) reach the percolation threshold. Pooyan et al. (2012) applied this model to predict the modulus of nanocomposites of cellulose acetate propionate (CAP) reinforced by cellulose nanowhiskers. According to this model, the effective elastic modulus (E_c) of the composite is defined as Eq. (12).

$$E_c = \frac{(1 - 2\psi + \psi v_f)E_m E_f + (1 - v_f)\psi E_f^2}{(1 - v_f)E_f + (v_f - \psi)E_m} \tag{12}$$

In which v_f, E_f, and E_m are fiber volume fraction, filler and matrix modulus, respectively. Ψ is an adjustable parameter according to Eq. (13).

$$\begin{cases} \psi = 0, & v_f \le v_{f_c} \\ \psi = v_f \left(\frac{v_f - v_{f_c}}{1 - v_{f_c}}\right)^b, & v_f > v_{f_c} \end{cases} \tag{13}$$

The parameter b describes the network density with a universal value of 0.4 for a three-dimensional fiber system (Pooyan et al. 2012). Term of v_{fc} corresponds to the critical volume fraction or percolation threshold that depends on the aspect ratio of reinforcing agent and its distribution within the matrix (Eq. 14).

$$v_{f_c} = \frac{0.7}{\frac{l}{d}} \tag{14}$$

where l and d are fiber length and diameter, respectively.

In above mentioned two models, modulus of CNF and PVA obtained by nanoindentation method is found to be 40 and 1.78 GPa (Table 2), respectively. As described earlier, in three-component nanocomposites, matrix is considered to be PVA/nHAp and CNF is as reinforcement. The aspect ratio of CNF is taken to be 100 (Fernandes et al. 2013). Since the density of CNF is 1.5 g/cm^3 (Pooyan et al. 2012), the fiber volume fraction is considered to be as fiber weight fraction.

The moduli of nanocomposites calculated by both models are presented in Table 3.

It can be noticed from Table 3 that the longitudinal modulus calculated using Halpin–Tsai model is in good agreement with the experimental value for PVA8/CNF3 nanocomposite, which suggests partial orientation of 3 wt% CNF within the electrospun fiber. Two other models provide a slightly lower agreement with experiments. By increasing filler content, the experimental values are closer to isotropic Halpin–Tsai modulus which can be due to random arrangement of fibers. This is more evident when nHAp is present in the matrix, even in the presence of a high shear field. Comparing the Halpin–Tsai modulus (E) with experimental data, it can be concluded that nanocomposites loaded by only 3 and 5 wt% CNF and also the one including 5 wt% CNF and small content of nHAp (1 wt%) have a better coincidence with this theoretical model. However, at high filler content (10 wt% nHAp and 3 wt%), there is more discrepancy. This effect can be attributed to the no filler–filler assumption in this model leading to better agreement at smaller filler content with less pronounced filler interactions. On the other hand, the predicted moduli by Ouali model matches better with experiment (6–7% difference) for three-component nanocomposites, while for PVA/CNF composites the discrepancy is 19–30%. As mentioned, Ouali model assumes that when interactions between fillers reach the percolation threshold, a rigid structure is formed. Therefore, better prediction of this model at higher contents of fillers and for three-component composites could be related to this assumption. In general, both models, particularly Ouali model, underestimate the experimental

Table 3 Comparison of nanocomposites modulus from models and experiments

Sample	Modulus					
	Matrix (E_m) (GPa)	Longitudinal Halpin–Tsai (E_L) (GPa)	Transverse Halpin–Tsai (E_T) (GPa)	Isotropic Halpin–Tsai (E) (GPa)	Ouali model (E) (GPa)	Experiment
PVA8/CNF3	1.78 ± 0.28	2.65	1.92	2.19	2.06	2.57 ± 0.59
PVA8/CNF5	1.78 ± 0.28	3.25	2.05	3.27	2.37	3.37 ± 0.47
PVA8/nHAp1/CNF5	12.73 ± 3.5	16.66	13.54	14.71	13.43	14.36 ± 2.72
PVA8/nHAp10/CNF3	15.74 ± 2.84	16.45	16.78	16.31	16.12	17.34 ± 3.46

results. Furthermore, Halpin–Tsai has better prediction at lower filler content and Ouali model at higher filler content and three-component composites.

Analysis of electrospun porous scaffolds: comparison with theoretical models

In order to have a prediction of mechanical behavior of electrospun mats and explore its relation to porosity, structural models are used. These models are based on cellular network structures, which were developed for high porosity structures. In such models, the modulus is a function of material porosity. In general, these models are mostly based on regular 2D or 3D packing (Shulmeister 1998; Srivastava and Srivastava 2014) in which the geometry of the considered unit cell plays the main role in model's equation. In these models, it is assumed that porosity is high (more than 70%), therefore they are suitable for nanofibrous scaffolds. Also, a single unit cell is representative of whole structure.

The simplest structural model is 2D honeycomb in which the unit cell is hexagonal. The effective modulus (E*) according to this model is presented by Eq. (15), where φ is the porosity and E is the modulus of solid (unfoamed) material (Thelen et al. 2004).

$$E^* = 1.4939E(1 - \varphi)^3 \tag{15}$$

In terms of 3D structures, two of the most widely used unit cells are cubic and tetrakaidecahedron (Fig. 4). The most comprehensive description of cubic model was given by Gibson and Ashby (Eq. 16) (Lee and Ramesh 2004; Srivastava and Srivastava 2014).

$$E^* = E(1 - \varphi)^2 \tag{16}$$

Another wide-spread model, based on the tetrakaidecahedron (Fig. 4), has been considered by several researchers, among them the most recent and more convenient one is the model developed by Zhu (Zhu et al. 1997) (Eq. 17).

$$E^* = \frac{0.726(1 - \varphi)^2}{1 + 1.09(1 - \varphi)} \tag{17}$$

The elastic modulus of porous scaffolds were calculated based on the above models and compared with experimental results obtained from tensile test in Table 4. The modulus of solid material is taken from AFM nanoindentation method.

According to Table 4, porosity plays a crucial role in mechanical stiffness of electrospun scaffolds. Due to the presence of high porosity, the tensile modulus decreases dramatically, which is proved by experiment as well as theoretical models. Moreover, all three models have an overestimated prediction of the modulus compared to experimental results. Among them, 2D honeycomb model has the best prediction for all samples. Between 3D models, tetrakaidecahedron model shows the best prediction for scaffolds with lower modulus, while discrepancy is larger for scaffolds with higher modulus. The worst prediction is given by the cubic model. One of the main assumptions in structural models is that single unit cell is representative of whole structure, so predictions of models in Table 4 are directly related to the shape of considered unit cells, which have hexagonal, cubic and tetrakaidecahedronal shapes. We believe that pores or unit cells in an electrospun scaffold are more similar to hexagons and tetrakaidecahedrons, so these models have a better prediction of measured modulus.

Fig. 4 Unit cells based on 3D models, Cubic (**a**) and Tetrakaidecahedron (**b**) model. Reproduced with permission from Lee and Ramesh (2004)
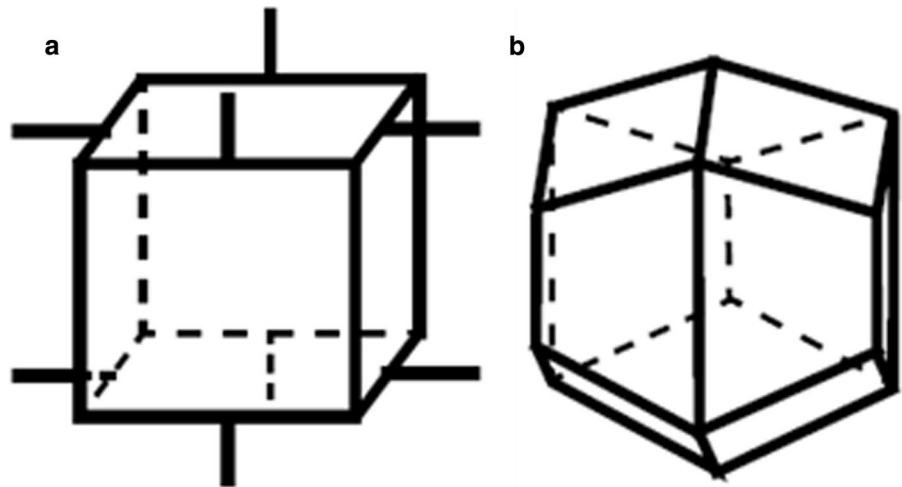

Table 4 Estimated modulus of electrospun scaffolds calculated from open-celled foam models

Sample	Property					
	E^a AFM (GPa)	Porosity (%)	Honeycomb model (MPa)	Cubic model (MPa)	Tetrakaidecahedron model (MPa)	Experiment (MPa)
PVA8	1.78 ± 0.28	80.4 ± 1.63	20.02	68.38	40.9	45.45 ± 4.77
PVA8/nHAp1	12.73 ± 3.5	79.84 ± 1.25	155.8	517.38	307.94	132.37 ± 26.09
PVA8/nHAp10	15.74 ± 2.84	79.02 ± 1.66	217	694.10	409.36	142.84 ± 7.1
PVA8/CNF3	2.57 ± 0.59	76.54 ± 1.23	49.57	141.40	81.77	76.3 ± 5.66
PVA8/CNF5	3.37 ± 0.47	76.10 ± 0.95	68.73	192.50	110.87	95.4 ± 7.46
PVA8/nHAp1/ CNF5	14.36 ± 2.72	78.65 ± 1.15	208.77	667.78	385.50	195.6 ± 13.5
PVA8/nHAp10/ CNF3	17.34 ± 3.46	75.39 ± 0.84	386.10	1050.2	601.18	322.9 ± 20.47

[a]This column shows the modulus of single fibers measured by AFM nanoindentation method

Conclusions

Electrospun PVA and its nanocomposites with different content of nHAp and CNF were successfully fabricated. Tensile test and AFM nanoindentaion were applied to measure the tensile modulus of electrospun scaffolds and electrospun single fibers respectively. In addition, theoretical models were used to predict the stiffness of nanocomposites and verify their accuracy by experimental data. For a single nanocomposite fiber, the Halpin–Tsai and Ouali models were used, while for the electrospun scaffolds, structural models related to open-celled structures were used. In general, Halpin–Tsai showed better agreement with the experiment than the Ouali model, especially at lower filler content. By increasing filler content, the Ouali model showed more conformity with experimental data. Due to high porous structure of all electrospun scaffolds (more than 70% porosity), a significant reduction of modulus were observed both from tensile tests and also theoretical predictions using structural models. Among structural models, honeycomb model provided the best prediction, while the cubic model predictions were the worst.

References

Abdalkarim SYH, Yu H-Y, Wang D, Yao J (2017) Electrospun poly(3-hydroxybutyrate-co-3-hydroxy-valerate)/cellulose reinforced nanofibrous membranes with ZnO nanocrystals for antibacterial wound dressings. Cellulose 24:2925–2938

Adibzadeh S, Bazgir S, Katbab AA (2014) Fabrication and characterization of chitosan/poly(vinyl alcohol) electrospun nanofibrous membranes containing silver nanoparticles for antibacterial water filtration. Iran Polym J 23:645–654

Agrawal P, Pramanik K (2016) Chitosan-poly(vinyl alcohol) nanofibers by free surface electrospinning for tissue engineering applications. Tissue Eng Regen Med 13:485–497

Baji A, Mai Y-W, Wong S-C, Abtahi M, Du X (2010) Mechanical behavior of self-assembled carbon nanotube reinforced nylon 6, 6 fibers. Compos Sci Technol 70:1401–1409

Barzegar F et al (2015) Preparation and characterization of poly(vinyl alcohol)/graphene nanofibers synthesized by electrospinning. J Phys Chem Solids 77:139–145

Bazbouz MB, Stylios GK (2010) The tensile properties of electrospun nylon 6 single nanofibers. J Polym Sci Part B Polym Phys 48:1719–1731

Costa-Júnior ES, Barbosa-Stancioli EF, Mansur AAP, Vasconcelos WL, Mansur HS (2009) Preparation and characterization of chitosan/poly(vinyl alcohol) chemically crosslinked blends for biomedical applications. Carbohydr Polym 76:472–481. https://doi.org/10.1016/j.carbpol.2008.11.015

Degirmenbasi N, Kalyon DM, Birinci E (2006) Biocomposites of nanohydroxyapatite with collagen and poly(vinyl alcohol). Colloids Surf B 48:42–49

Dong G et al (2010) Preparation and characterization of Ag nanoparticle-embedded polymer electrospun nanofibers. J Nanoparticle Res 12:1319–1329

Enayati MS et al (2016a) Fabrication and characterization of electrospun bionanocomposites of poly(vinyl alcohol)/nanohydroxyapatite/cellulose nanofibers. Int J Polym Mater Polym Biomater 65:660–674

Enayati MS et al (2016b) Crystallinity study of electrospun poly(vinyl alcohol) nanofibers: effect of electrospinning, filler incorporation, and heat treatment. Iran Polym J 25:647–659

Fallahiarezoudar E, Ahmadipourroudposht M, Yusof NM, Idris A (2015) Influence of process factors on diameter of core (γ-Fe$_2$O$_3$)/shell poly(vinyl alcohol) structure magnetic nanofibers during co-axial electrospinning. Int J Polym Mater Polym Biomater 64:15–24

Fernandes EM, Pires RA, Mano JF, Reis RL (2013) Bionanocomposites from lignocellulosic resources: properties, applications and future trends for their use in the biomedical field. Prog Polym Sci 38:1415–1441

Halpin JC (1992) Primer on composite materials analysis (Revised). CRC Press, London

Inai R, Kotaki M, Ramakrishna S (2005) Structure and properties of electrospun PLLA single nanofibres. Nanotechnology 16:208

Islam MS, Rahaman MS, Yeum JH (2015) Electrospun novel super-absorbent based on polysaccharide–poly(vinyl alcohol)–montmorillonite clay nanocomposites. Carbohydr Polym 115:69–77

Khalf A, Singarapu K, Madihally SV (2015) Cellulose acetate core–shell structured electrospun fiber: fabrication and characterization. Cellulose 22:1389–1400

Kim G-M, Asran AS, Michler GH, Simon P, Kim J-S (2008) Electrospun PVA/HAp nanocomposite nanofibers: biomimetics of mineralized hard tissues at a lower level of complexity. Bioinspir Biomim 3:046003

Koosha M, Mirzadeh H, Shokrgozar MA, Farokhi M (2015) Nanoclay-reinforced electrospun chitosan/PVA nanocomposite nanofibers for biomedical applications. RSC Adv 5:10479–10487

Kumar V, Rawal A (2017) Elastic moduli of electrospun mats: importance of fiber curvature and specimen dimensions. J Mech Behav Biomed Mater 72:6–13

Lee J, Deng Y (2013) Nanoindentation study of individual cellulose nanowhisker-reinforced PVA electrospun fiber. Polym Bull 70:1205–1219

Lee S-T, Ramesh NS (2004) Polymeric foams: mechanisms and materials. CRC Press, London

Linh NTB, Lee B-T (2012) Electrospinning of poly(vinyl alcohol)/gelatin nanofiber composites and cross-linking for bone tissue engineering application. J Biomater Appl 27:255–266

Linh B, Thuy N, Lee KH, Lee BT (2013) Functional nanofiber mat of poly(vinyl alcohol)/gelatin containing nanoparticles of biphasic calcium phosphate for bone regeneration in rat calvaria defects. J Biomed Mater Res Part A 101:2412–2423

Liu W, Yee S, Adanur S (2014) Properties of electrospun PVA/nanoclay composites. J Text Inst 105:423–429

Ma L, Wang L, Wu L, Zhuo D, Weng Z, Ren R (2014) Cellulosic nanocomposite membranes from hydroxypropyl cellulose reinforced by cellulose nanocrystals. Cellulose 21:4443–4454

Mehrasa M et al (2016) Incorporation of zeolite and silica nanoparticles into electrospun PVA/collagen nanofibrous scaffolds: the influence on the physical, chemical properties and cell behavior. Int J Polym Mater Polym Biomater 65:457–465

Meng Z, Wang Y, Ma C, Zheng W, Li L, Zheng Y (2010) Electrospinning of PLGA/gelatin randomly-oriented and aligned nanofibers as potential scaffold in tissue engineering. Mater Sci Eng C 30:1204–1210

Neisiany RE, Khorasani SN, Naeimirad M, Lee JKY, Ramakrishna S (2017a) Improving mechanical properties of carbon/epoxy composite by incorporating functionalized electrospun polyacrylonitrile nanofibers. Macromol Mater Eng. https://doi.org/10.1002/mame.201600551

Neisiany RE, Lee JKY, Khorasani SN, Ramakrishna S (2017b) Towards the development of self-healing carbon/epoxy composites with improved potential provided by efficient

encapsulation of healing agents in core-shell nanofibers. Polym Test 62:79–87

Ouali N, Cavaillé J, Perez J (1991) Elastic, viscoelastic and plastic behavior of multiphase polymer blends. Plast Rubber Compos Process Appl (UK) 16:55–60

Persano L, Camposeo A, Tekmen C, Pisignano D (2013) Industrial upscaling of electrospinning and applications of polymer nanofibers: a review. Macromol Mater Eng 298:504–520. https://doi.org/10.1002/mame.201200290

Pierini F, Lanzi M, Nakielski P, Pawłowska S, Zembrzycki K, Kowalewski TA (2016) Electrospun poly(3-hexylthiophene)/poly(ethylene oxide)/graphene oxide composite nanofibers: effects of graphene oxide reduction. Polym Adv Technol 27:1465–1475

Pon-On W, Charoenphandhu N, Teerapornpuntakit J, Thongbunchoo J, Krishnamra N, Tang I-M (2014) Mechanical properties, biological activity and protein controlled release by poly(vinyl alcohol)–bioglass/chitosan–collagen composite scaffolds: a bone tissue engineering applications. Mater Sci Eng C 38:63–72

Pooyan P, Tannenbaum R, Garmestani H (2012) Mechanical behavior of a cellulose-reinforced scaffold in vascular tissue engineering. J Mech Behav Biomed Mater 7:50–59

Ramakrishna S, Lim T, Inai R, Fujihara K (2006) Modified Halpin–Tsai equation for clay-reinforced polymer nanofiber. Mech Adv Mater Struct 13:77–81

Sambudi NS, Sathyamurthy M, Lee GM, Park SB (2015) Electrospun chitosan/poly(vinyl alcohol) reinforced with CaCO$_3$ nanoparticles with enhanced mechanical properties and biocompatibility for cartilage tissue engineering. Compos Sci Technol 106:76–84

Sheikh FA, Barakat NA, Kanjwal MA, Park SJ, Park DK, Kim HY (2010) Synthesis of poly(vinyl alcohol) (PVA) nanofibers incorporating hydroxyapatite nanoparticles as future implant materials. Macromol Res 18:59–66

Shokrollahi M, Morshed M, Semnani D, Rezaei B (2014) Development of electro-spun poly(vinyl alcohol)/titanium dioxide membrane-based polymer electrolytes for lithium–ion batteries. Int J Polym Mater Polym Biomater 63:161–171

Shulmeister V (1998) Modelling of the mechanical properties of low-density foams. Dissertation, Delft University of Technology

Srivastava V, Srivastava R (2014) On the polymeric foams: modeling and properties. J Mater Sci 49:2681–2692

Stachewicz U, Bailey RJ, Wang W, Barber AH (2012) Size dependent mechanical properties of electrospun polymer fibers from a composite structure. Polymer 53:5132–5137

Tan E, Lim C (2004) Physical properties of a single polymeric nanofiber. Appl Phys Lett 84:1603–1605

Tan E, Goh C, Sow C, Lim C (2005) Tensile test of a single nanofiber using an atomic force microscope tip. Appl Phys Lett 86:073115

Thelen S, Barthelat F, Brinson LC (2004) Mechanics considerations for microporous titanium as an orthopedic implant material. J Biomed Mater Res Part A 69:601–610

Usov I et al (2015) Understanding nanocellulose chirality and structure–properties relationship at the single fibril level. Nat Commun 6:7564

Wang W, Barber AH (2012) Measurement of size-dependent glass transition temperature in electrospun polymer fibers using AFM nanomechanical testing. J Polym Sci Part B Polym Phys 50:546–551

Wang C, Li Y, Ding G, Xie X, Jiang M (2013) Preparation and characterization of graphene oxide/poly(vinyl alcohol) composite nanofibers via electrospinning. J Appl Polym Sci 127:3026–3032

Xiao S, Gao R, Gao L, Li J (2016) Poly(vinyl alcohol) films reinforced with nanofibrillated cellulose (NFC) isolated from corn husk by high intensity ultrasonication. Carbohydr Polym 136:1027–1034

Yang E, Qin X, Wang S (2008) Electrospun crosslinked poly(vinyl alcohol) membrane. Mater Lett 62:3555–3557

Zhu H, Knott J, Mills N (1997) Analysis of the elastic properties of open-cell foams with tetrakaidecahedral cells. J Mech Phys Solids 45:319327–325343